Calibration of high accuracy accelerometers for ESA missions BepiColombo and JUICE at INRIM

Calibration of high accuracy accelerometers for ESA missions BepiColombo and JUICE at INRIM

OPEN ACCESS
IOP Publishing
Measurement Science and Technology
Meas. Sci. Technol. **34** (2023) 104001 (9pp)
https://doi.org/10.1088/1361-6501/ace20c

Calibration of high accuracy accelerometers for ESA missions BepiColombo and JUICE at INRIM

Milena Astrua*, Marco Pisani, Marco Santiano and Emanuele Audrito

INRIM, Istituto Nazionale di Ricerca Metrologica, Strada delle Cacce, 91, Torino, 10135, Italy

E-mail: m.astrua@inrim.it

Received 15 January 2023, revised 23 June 2023
Accepted for publication 27 June 2023
Published 6 July 2023

Abstract

High sensitive triaxial accelerometers are used in several space missions to measure the non-gravitational accelerations acting on the spacecraft. Among these, the capacitive accelerometers developed for ESA missions Jupiter Icy moons Explorer (JUICE) and BepiColombo were designed to measure accelerations of the order of $3 \cdot 10^{-6}$ m s^{-2} with an accuracy level of 300 ppm in the frequency range ($3 \cdot 10^{-5}$–0.1) Hz. Despite the signal to be measured is of the same order of magnitude of the seismic noise on the earth, an accurate on-ground calibration is needed. The facility set-up at INRIM to this purpose is based on a simple principle: the base of the accelerometer is dynamically tilted by an angle α so that the sensor undergoes a component of the gravitational acceleration g proportional to angle α. In practice, several issues have to be addressed by the calibration facility, such as the seismic noise limiting the signal-to-noise ratio, the generation and the accurate measurement of the tilt angle. Furthermore, the calibration was performed taking into account different on-flight conditions such as different operating temperatures and possible deformation of the accelerometers during the launch. The experimental set-up and the calibration procedure are described in the paper. The measurement results and the uncertainty budget show that a relative accuracy of 240 ppm has been achieved.

Keywords: capacitive accelerometer, calibration, BepiColombo, JUICE, HAA, ISA

(Some figures may appear in colour only in the online journal)

1. Introduction

Triaxial accelerometers are essential instruments for every spacecraft. They are used to measure the spacecraft roll, the satellite altitude or even the atmosphere density during the satellite deceleration caused by the aerodynamic drag. Some space missions devoted to the Earth's observation or to interplanetary investigations require extremely high sensitivity accelerometers to measure the non-gravitational accelerations induced by direct solar radiation or by thermal emission from the planet, in order to correct the spacecraft orbit and precisely measure the gravitational field of the planet.

In case of space missions dedicated to map the Earth's gravity field, such as gravity recovery and climate experiment (GRACE) or gravity field and steady-state ocean circular explorer (GOCE), the calibration of accelerometers can be performed on-board by means of GPS-based orbit determination [1, 2]. This procedure is not possible for accelerometers on-board of interplanetary missions.

As an example, high accuracy accelerometer (HAA) is integrated in the radio science experiment of JUICE (Jupiter Icy moons Explorer) mission, with the aim of studying the gravity field of Ganymede, the extent of the internal ocean on the icy moons and the structure of the atmosphere of Jupiter and its moons [3]. Another example can be found in

* Author to whom any correspondence should be addressed.

the joint mission between the European Space Agency (ESA) and the Japan Aerospace Exploration Agency (JAXA), named BepiColombo, devoted to the measurement of the gravitational field and rotational state of Mercury, which hosts a radio science experiment based on Italian Spring Accelerometer (ISA) [4].

In order to reach the objectives of the experiments of ESA missions, these sensors have been designed to measure accelerations as small as $3 \cdot 10^{-6}$ m s^{-2} with an accuracy level of 300 ppm in the frequency range ($3 \cdot 10^{-5}$–0.1) Hz. Since the signal to be measured is of the same order of magnitude of the seismic noise on the earth, the necessary on-ground calibration is a challenging issue.

The accelerometers used in JUICE and BepiColombo missions have been manufactured by Thales Alenia Space Italia (TAS-I), according to the design and the targeted performance presented in [5]. The sensors are based on three single axis accelerometers arranged along the three Cartesian axes. Each accelerometer is a spring-mass system made of a moving mass connected to the frame by a tiny blade acting as the spring. A couple of plates (named pick-up plates) faces the mass so to form two equal capacitors at the two sides of the mass which are read by a bridge capacimeter. When the mass moves the capacitance change is read by the bridge which gives an electrical signal proportional to the displacement of the proof mass. In fact, each accelerometer behaves as a damped harmonic oscillator with its peculiar transfer function. The knowledge of the transfer function allows to convert the displacement of the mass, measured by the capacitors, into the acceleration which caused the displacement. The point is that the transfer function may change due to, for example, shock from the launch of the satellite that could change the elastic constant of the spring. Therefore a method to recalibrate the device in orbit is necessary. To the purpose, a second couple of electrostatic plates (actuators) has been arranged to face the mass and impose to it a known force by means of variable voltages. This feature will allow the on-flight calibration of pick-up plates. Moreover, in case the shock due to the launch had caused a bending of the spring, the actuators allow to force the position of the mass to work in the zero electrical position, in order to avoid non linearity effect and to exploit the whole electrical dynamic range of the sensor. A last function of the actuators is to reduce the constant of the mechanical spring by applying an attractive force between the mass and the plates as described in the next section.

A detailed description of the working principle of accelerometers developed for BepiColombo can be found in [6]. In [7] can be found further details on the triaxial ISA accelerometer and the first measurements from the satellite in-flight towards Mercury. Based on the gained experience, a second generation of accelerometers was later manufactured for the JUICE mission.

The calibration strategy and the facility set up at INRIM to calibrate these accelerometers are described in sections 2–4, the calibration procedure adopted is illustrated in section 5 while the main results and the uncertainty budget are outlined in section 6.

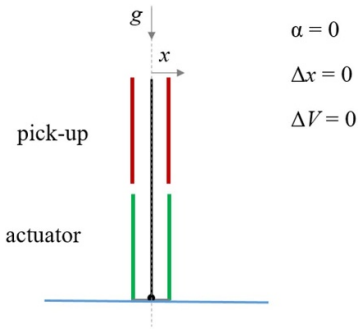

Figure 1. Schematic representation of the accelerometer in equilibrium condition.

2. Calibration strategy

The relationship between the voltage applied to the actuators and the corresponding acceleration value is the aim of the on-ground calibration. To this purpose, a facility able to generate a known and traceable acceleration has been designed. The principle is described in [8] and consists in tilting the accelerator base by a known angle α so that the proof mass undergoes an acceleration a proportional to the gravitational acceleration g according to the following formula:

$$a = g \cdot \sin(\alpha) \approx g \cdot \alpha, \text{for small angles.} \quad (1)$$

A schematic representation of the accelerometer in equilibrium condition is presented in figure 1.

The pick-up plates are drawn in red, while the actuator plates are in green; the proof mass is represented by a black solid line, fixed to the frame through a tiny blade represented by a black dot. The sensor is arranged in inverse pendulum configuration (i.e. the proof mass is above the blade).

In equilibrium condition, the proof mass is aligned with the local gravitational acceleration g ($\alpha = 0$), hence there is no displacement caused by acceleration ($\Delta x = 0$) and no voltage difference between the actuators ($\Delta V = 0$).

The calibration procedure is divided into two steps.

In the first step, the base of the accelerometer is tilted by an angle $\alpha = \alpha_n$ so the sensor undergoes an acceleration equal to $a = g \cdot \alpha$ that causes a mass displacement $\Delta x = x_n$ with respect to the rest position, as represented in figure 2. This configuration allows to find the relationship between the applied acceleration, a, and the signal coming from the pick-up sensor, $S = S(a)$.

In the second step, the base of the accelerometer is again horizontal ($\alpha = 0$) and a voltage difference between the actuators $\Delta V = V_n$ is applied; this causes a displacement of the proof mass as represented in figure 3. The applied voltage unbalance is trimmed to cause a displacement similar to the one due to the acceleration x_n.

Therefore, the calibration is obtained comparing the voltage difference applied to the actuators, V_n, with the signal from the pick-up sensor, which in turn is linked to the acceleration by means of the relationship $S = S(a)$. Eventually, the output of the calibration process is the ratio between the

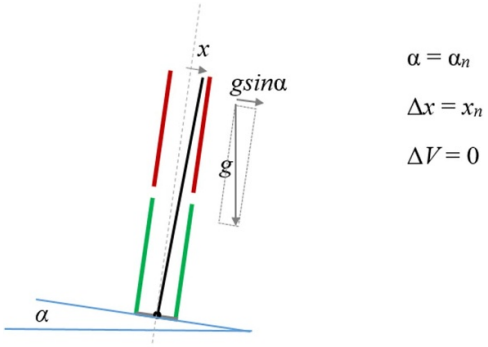

Figure 2. Schematic representation of the accelerometer tilted by an angle α (the tilt is magnified for the sake of clarity).

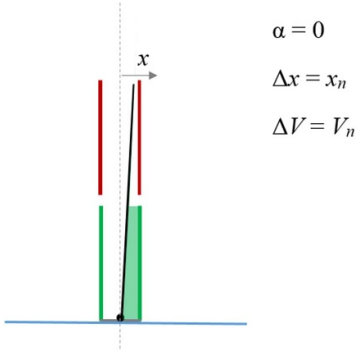

Figure 3. Schematic representation of the accelerometer with horizontal base and voltage difference between the actuators.

acceleration and the voltage applied to the actuators in units m s^{-2} V^{-1}.

The force acting on the proof mass, due to the voltages V_{a1} and V_{a2} on the actuator plates, can be described by equation (2):

$$F = 0.5\varepsilon_0 A \left[\frac{V_{a2}^2}{(d_0 - x)^2} - \frac{V_{a1}^2}{(d_0 + x)^2} \right] \tag{2}$$

where ε_0 is the vacuum dielectric constant, A is the actuator plate area, d_0 is the distance between the mass and the actuator plate and x is the actual displacement of the proof mass from the equilibrium. If the mass displacement is much less than the distance d_0, and neglecting the non-parallelism between the plates, equation (2) can be simplified as follows:

$$F = \frac{\varepsilon_0}{d_0^3} A \left(V_{a2}^2 + V_{a1}^2 \right) \cdot x - \frac{\varepsilon_0}{2d_0^2} A \left(V_{a2}^2 - V_{a1}^2 \right). \tag{3}$$

The first contribution in equation (3) represents the electrical contribution to the elastic constant of the harmonic oscillator that allows to lower the resonant frequency of the test mass down to 3.5 Hz.

The second contribution causes a displacement of the sensing mass which is attracted by the actuator plate with the higher voltage.

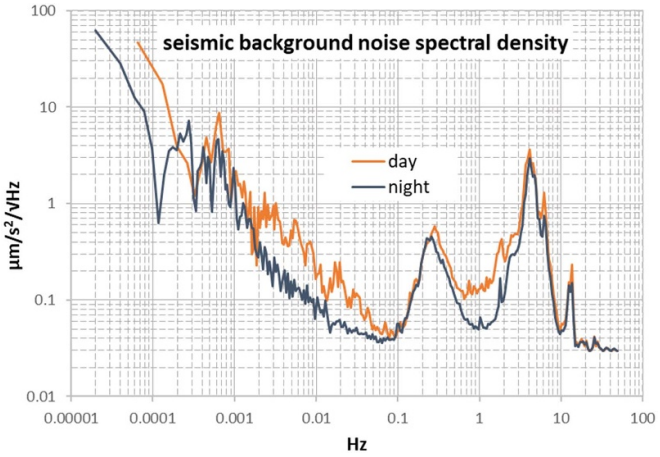

Figure 4. Noise spectral density of the typical background seismic acceleration expressed in μm s^{-2} $\sqrt{\text{Hz}^{-1}}$ measured at INRIM. Two measurements are taken during day and night. The 'bump' around 0.25 Hz is the typical acceleration due to the sea waves striking the coasts, the peak around 4 Hz is due to the resonance frequency of the accelerometer used for the measurements. The lowest noise level is achieved between 0.01 and 0.1 Hz.

3. Dynamic calibration

The above description refers to the hypothesis of a static calibration as suggested in [8]. In fact, due to the presence of seismic noise and the request of an accuracy level of 300 ppm, it is not possible to perform the calibration at discrete tilt angles from the horizontal plane. The point is that in a real laboratory environment placed on the Earth, a background seismic noise is always present because of a number of natural and artificial sources such as tidal motions, sea waves, meteorological movements, anthropogenic sources each one acting in different spectral regions. This behaviour is well known and, although it depends on the specific location on the Earth, it shows common features extensively described in [9] where background seismic noise is collected from many sources around the world. A more specific model can be found in [10] where the average spectral noise in northern Italy is analysed. From these analysis is evident that the acceleration of the Earth's crust is larger than the working range of HAA or ISA (few micrometres per squared second) except for a specific range of frequencies. Indeed the natural vibrations decrease with frequency up to about 0.01 Hz where it reaches a noise density level lower than 100 nm s^{-2} $\sqrt{\text{Hz}^{-1}}$, then it increases again around 0.1 Hz showing a typical peak between 0.1 and 1 Hz mainly due to the sea waves hitting the coasts. In figure 4 is shown a measurement of the seismic background noise performed on the granite optical table, devoted to angle metrology, used for the calibration of HAA. The spectra are compliant with the ones described in [9, 10].

For the above reason instead of a static calibration (at zero frequency) of the accelerometers, a dynamic mode was chosen. The best signal to noise ratio can be obtained in the range between 0.01 and 0.1 Hz. In this interval the working frequency was chosen taking into account two factors: the first is that the more we are far from the resonant frequency

the more the calibration can be considered equivalent to a static one; the second is that each measurement needs the averaging of many cycles in order to increase the signal to noise (S/N) ratio, so higher frequencies mean faster measurements. The last point to be assessed is the amplitude of the stimulus considering that larger signals increase the S/N, but too large displacement could affect the linearity of the system.

On the base of the above considerations, in agreement with TAS-I, it was decided to perform the calibration in a dynamical regime by applying a sinusoidal modulation with frequency equal to 50 mHz and angular amplitude about 150 microradians corresponding to about 10^{-3} m s^{-2}. Thus the signal analysis will be performed in the frequency domain by measuring the amplitude of peaks in the FFT spectra of the accelerometer output. Afterwards, the actuators are excited by a periodical signal at the same frequency, in order to generate a periodic displacement of the mass with the same amplitude. Further details on this topic can be found in [11, 12].

After the launch and when the accelerometers will be in-flight, because of the shock and vibrations effects on the blade, the position where the sensing mass will go without gravity could change with respect to the position on-ground, up to 10 μm. This shift in the mass position represents a serious problem, since the accelerometers must work with the sensing mass in zero electrical position, in order to use all the electrical dynamic range and to avoid non-linearity effects. To solve this issue, a suitable unbalancing of the actuators voltage allows to force the sensing mass again in the zero electrical position. It is difficult to model the effect of the unbalance of the voltages on the calibration factor, so it was decided to perform the calibration also in these non-ideal conditions. This is simulated by tilting the whole structure by a constant value as described in section 5.

4. Experimental set-up

The facility was set-up in 2014, for the calibration of accelerometers for BepiColombo mission [12] and next upgraded in 2020 for the calibration of accelerometers to be used in JUICE mission. The following description refers to the more recent and optimized set-up aimed at the calibration of HAA.

As previously stated, the calibration is based on a tilt of the accelerator base by a known angle α, in order to generate an acceleration equal to $g{\cdot}\alpha$.

Furthermore it is expected that the calibration factors are temperature dependent. Thus, since it is foreseen that the HAA accelerometer will operate in a temperature range between 30 °C and 50 °C, it is necessary to perform the calibration at different temperatures. To this purpose, the accelerometers were placed inside a special designed thermostated aluminium box. The box was mounted on a structure with three arms of the same height to support the structure on three points (sphere on plane). Two arms stand on fixed pillars, while the third is moved by a piezoelectric actuator so that the whole structure can be tilted by an electrical signal to calibrate one accelerometer at a time. Rotating the box by 90° with respect to the three support points, it is possible to test all three accelerometers.

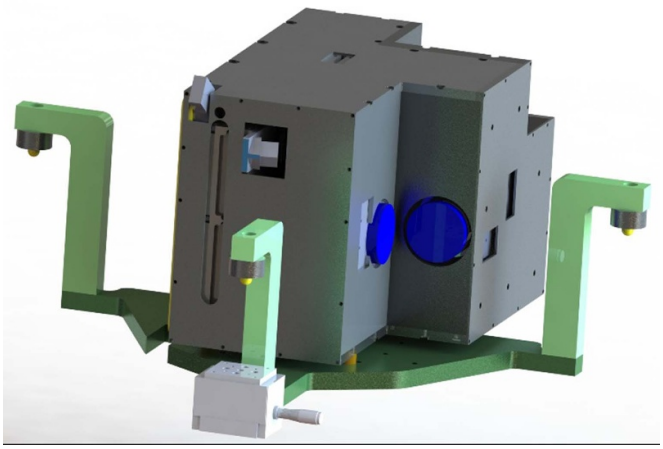

Figure 5. CAD model of the pivoting structure. In grey the thermally stabilized box containing the accelerometers. In blue the mirrors glued to the accelerometers shrouds used to measure the tilt angles. In green the tilting base resting on three spheres. Two spheres act as pivoting points defining a rotating axis; the third one is moved up and down by the piezo actuator.

It is worth to note that the arms height is studied so that the rotation axis passes through the centre of the accelerometer under test. The CAD model of the pivoting structure and the aluminium box containing the accelerometers are shown in figure 5.

The piezoelectric actuator has been realized with mechanically amplified piezoelectric actuators manufactured by Cedrat Technologies, model APA 60S. The piezoelectric elongation is modulated by a sinusoidal signal at 50 mHz and generates a stroke of about 50 μm, corresponding to an angle of about 150 μrad p.p. The modulating signal coming from a synthesiser (RIGOL, model DG4162) is amplified by an LVPZT-Amplifier module, manufactured by PI (Physik Instrumente).

The piezoelectric actuator, made of three units driven in parallel, manages to bear high loads (of the order of some kilograms) with good linearity and repeatability. A picture of the piezoelectric actuator is shown in figure 6.

A high flatness mirror was fixed to the outer shell of each accelerometer by means of a vacuum compliant adhesive tape. These mirrors are visible from the outside of the aluminium box through three apertures. A high precision autocollimator (AC) was aligned to face the mirror of the accelerometer under test to measure the rotation angle generated by the piezoelectric elongation. This measurement is a crucial point of the procedure. The autocollimator is based on a Hilger and Watts TA-5 model modified to enhance its performance and fit to the present purpose. The original detection system in the focal plane of the optical system of the autocollimator was replaced by a CCD camera, connected to a computer. The images coming from the mirror fixed to the accelerometer are analysed by

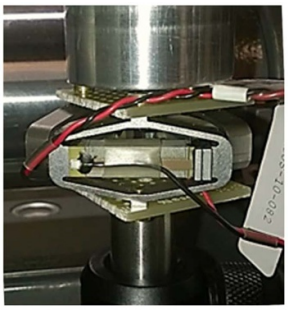

Figure 6. Picture of the three piezoelectric actuators arrangement used to tilt the accelerometers with a sinusoidal signal.

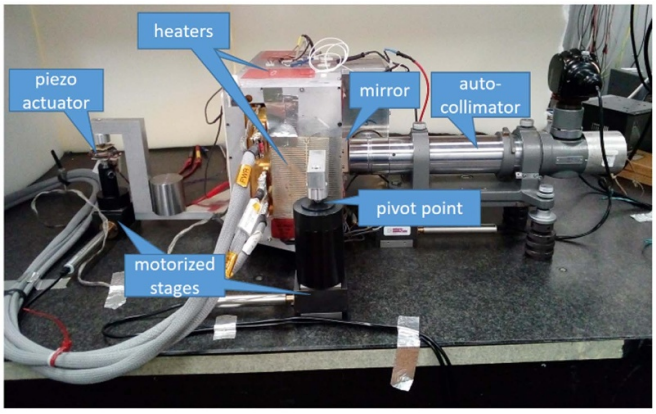

Figure 7. Picture of the experimental set-up for the calibration of JUICE HAA, FMz accelerometer.

a software implemented in LabVIEW® to obtain the information on the rotation angle of the accelerometer. The measuring range of the instrument is 500″ with an angular resolution of 0.01″. Moreover, the camera can be triggered by an external signal, in order to allow an accurate spectral analysis of the signals. The autocollimator was calibrated with respect to the national angle standard at INRIM [13] in order to ensure the traceability of the angle measurement to SI units. As a results of the calibration procedure, the angle sensitivity of the autocollimator was measured equal to 1.6921 px arcsec^{-1} with a relative uncertainty equal to $1.0 \cdot 10^{-4}$ on a measurement range of 150 μrad. Further details on the autocollimator performances and calibration can be found in [14].

A picture of the experimental set-up for the calibration of the HAA, flight model, z-axis (FMz) accelerometer for JUICE is shown in figure 7.

The aluminium box containing the accelerometers is equipped with heaters that allow to stabilize the environment at different temperatures. Heaters are divided in three groups, each one connected to a temperature controller (Lakeshore, model 330 or 340) equipped with a platinum resistance thermometer in contact with the box wall. A LabVIEW® program allows to adjust the temperature setpoint and the PID parameters for each controller, ensuring a temperature stability within ±0.02 °C.

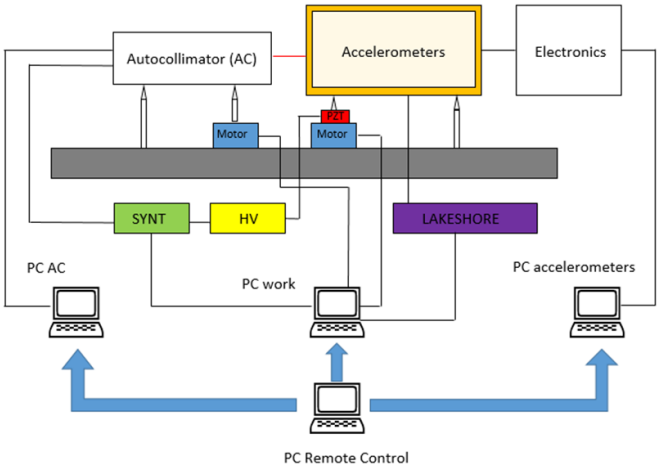

Figure 8. Block diagram of the calibration set-up.

The whole calibration set-up is controlled by four PCs connected via LAN. The block diagram of the whole calibration set-up is shown in figure 8.

The computer named ‘PC AC’ handles the autocollimator for the measurement of the tilt angle at a frequency of 2 Hz, triggered by a signal coming from the synthesiser (SYNT). This PC is also used at the end of a measuring run to analyse the calibration data in terms of Fourier analysis.

A second computer (‘PC accelerometers’) provided by TAS-I is entirely dedicated to the accelerometers: all the signals and controls acting on the accelerometers are managed by a closed digital control unit present on this PC. Indeed, the voltage settings and measurements are embedded in the electronics of the accelerometers, so that they can be considered as fully digital sensors. An input control panel allows to set the nominal voltage values of each actuator.

A third computer (‘PC work’) is used to control several processes: (i) the motorised screws (Motor) to adjust the vertical alignment of the autocollimator and accelerometer, (ii) the synthesiser (SYNT) to generates the sinusoidal signal for the piezoelectric actuator and the trigger signal for the acquisition of the autocollimator; (iii) the temperature controllers (LAKESHORE) for thermostating the box with the accelerometers.

All these PCs are controlled by a fourth computer (‘PC Remote Control’), in order to perform all the calibration remotely without the need for an operator in the laboratory.

5. Calibration procedure

As previously stated, each single calibration point is divided in two steps:

(1) Calibration of the pick-up response to the acceleration generated by g and α
(2) Calibration of the pick-up response to the stimulus generated by the actuators.

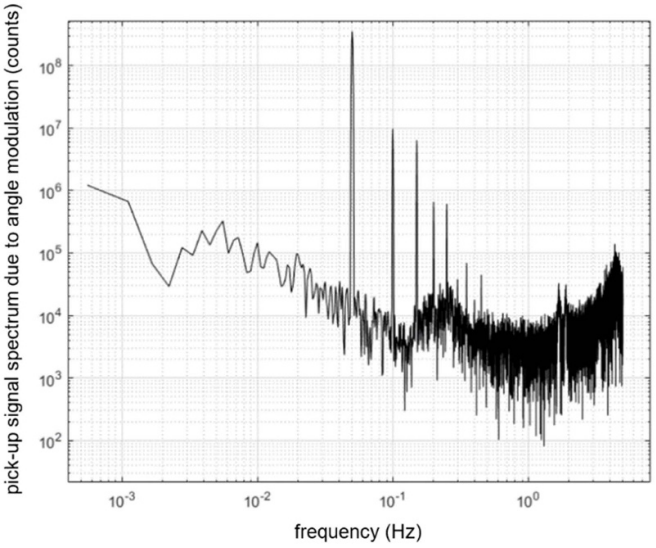

Figure 9. Spectrum of the pick-up signal due to the angle modulation.

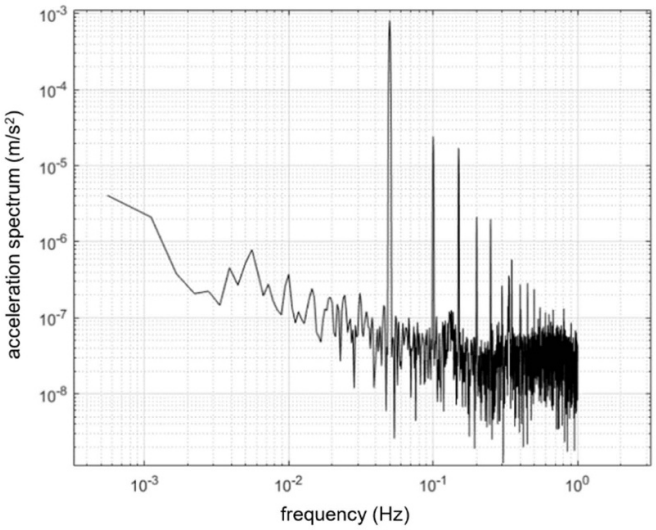

Figure 10. Spectrum of the autocollimator signal multiplied by the gravitational acceleration value used as the reference for the calibration procedure.

In the first step, the elongation of the piezoelectric actuator is modulated by a sinusoidal signal at a frequency of 50 mHz, in order to generate an angle of about 150 μrad p.p. The modulation lasts as long as necessary so that the first peak of the accelerometer and autocollimator signal spectra is at least four order of magnitude above the noise (about 20 min).

The spectrum of the pick-up signal expressed in counts is shown in figure 9: the peak at 50 mHz due to the angle modulation and its harmonics are clearly visible. The vertical scale is in 'counts' of the digital unit which elaborates the signals from the pick-up. The little bump observed around 0.25 Hz is due to the seismic noise as well as the increase at low frequency. Other sources of noise contributing to the spectrum are the actuator voltage noise and stability. Likewise, the spectrum of the autocollimator, multiplied by the gravitational acceleration value to be expressed in m s^{-2}, is shown in figure 10. This signal is the reference value used for the calibration.

The ratio between the peak of the accelerometer signal and the corresponding peak of the autocollimator provides the conversion factor, i.e. the relationship between the applied acceleration (in m s^{-2}) and the signal coming from the pick-up sensor (in counts).

Then, in the second step, the actuators are activated with a voltage modulation V_{mod} in order to move the sensing mass according to a square wave with period and amplitude close to the sine wave in point (1). The corresponding spectrum of the pick-up signal is calculated and shown in figure 11. It is evident the high harmonic content of this spectrum with respect to the previous ones due to the different nature of the driving signals. For the calibration only the fundamental line is considered.

Finally, the first peak of the accelerometer signal obtained at point (2) is multiplied by the conversion factor obtained at point (1) to provide the relationship between the acceleration and the applied voltage V_{mod}.

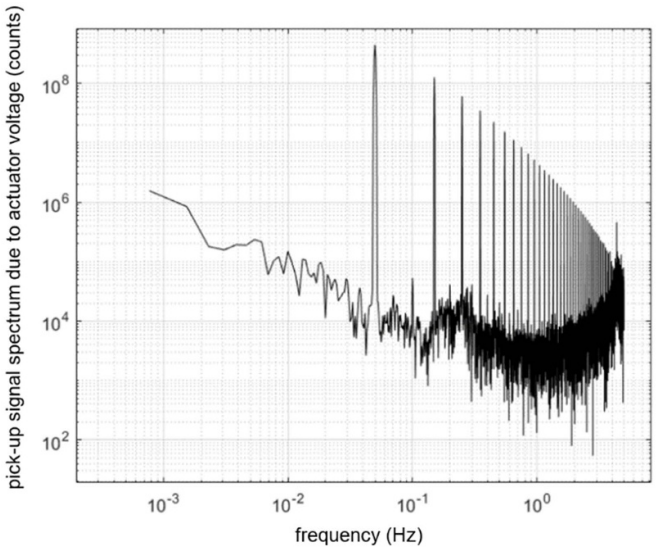

Figure 11. Spectrum of the pick-up signal due to the excitation of the actuator plates.

The second step of the calibration should follow the first one promptly, in order to ensure that the elastic constant of the harmonic oscillator, or other experimental conditions, do not change between the two steps.

Then, the calibration is carried out in unbalanced conditions to take into account the possibility of a deformation of the elastic hinge caused by shock and vibrations undergone at the moment of the launch that must be compensated with an unbalance of the actuators' voltage. In order to simulate this condition a constant tilt is applied to the accelerometer, through a motorized actuator, to move the plate from the balanced condition, contextually the voltage of the actuators is

unbalanced to return the mass into the central position. In this new condition the calibration procedure described above is repeated and a new calibration factor is obtained. As example, when the accelerometer base is tilted by 240 μrad, the mass displacement with respect to the central position is 4 μm. In order to centre again the proof mass, the farer actuator should be excited with a DC voltage $V_1 = 68.4$ V. Since, as described in section 2, we must respect the constraint on the sum of the squared voltages, the second actuator voltage V_2 will be $V_2 = \sqrt{(66)^2 - (68.4)^2} = 63.509\,36$ V (see formula (3)). This procedure is repeated for seven different actuator positions, always respecting the constraint on the sum of the squared voltages, in order not to change the elastic constant of the harmonic oscillator along the whole calibration procedure. The measurement at 66 V (central point) is repeated several times during the measurement sequence, in order to check the mechanical and thermal stability. Finally we manage to obtain a calibration curve which takes into account all the possible working conditions of the accelerometer.

In the end, in order to characterize the accelerometer for any possible temperature condition in-flight, the whole calibration process has to be repeated at different temperatures in the range between 30 °C and 50 °C, which is the maximum temperature range that accelerometers will face in flight.

6. Measurement results and uncertainty

We have performed seven calibration points for each temperature conditions. The measuring steps were chosen in order to measure the calibration factor for a mass displacement equal to ±4 μm, ±8 μm and ±10 μm with respect to the central position.

Typical calibration curves of JUICE FMx accelerometer at three different temperature conditions and sum of squared voltages equal to 8712 V^2 are shown in figure 12. Each measurement point shown in figure 12 was obtained with the two-steps procedure described in section 5. The measurement at the central point (66 V) was repeated several times during the measurement sequence, in order to check the mechanical and thermal stability. A repeatability of 70 ppm was obtained.

As expected from theory, the accelerometer's sensitivity shows a second order non-linearity, so the calibration curve can be described and interpolated by a second order polynomial

$$f(V_a) = AV_a^2 + BV_a + C \tag{4}$$

where *A, B* and *C* coefficients are the calibration results.

Figure 12 clearly shows that the calibration factor of accelerometers is heavily influenced by temperature. This effect is due to the thermal expansion coefficient of materials the accelerometers are made of. To minimize the effect of temperature on the measurement of the accelerometers, these sensors are mounted in the inner part of the satellite which is thermally controlled, nevertheless the effect of temperature must be accurately evaluated.

The thermal sensitivity can be estimated by a linear interpolation of the calibration factor values at 66 V with respect

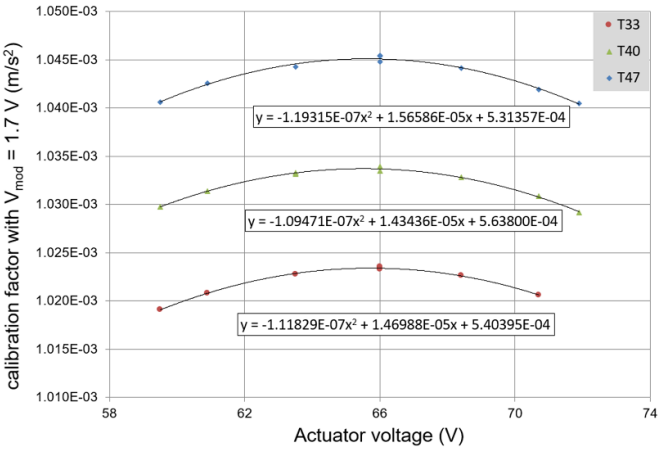

Figure 12. Calibration curves of JUICE FMx accelerometer in different temperature conditions. The horizontal axis is the voltage of one of the two electrodes (the voltage of the second one is complementary to the first). Note that the measurement points at 33 °C are only 6, because the result obtained at 72 V was considered an outlier.

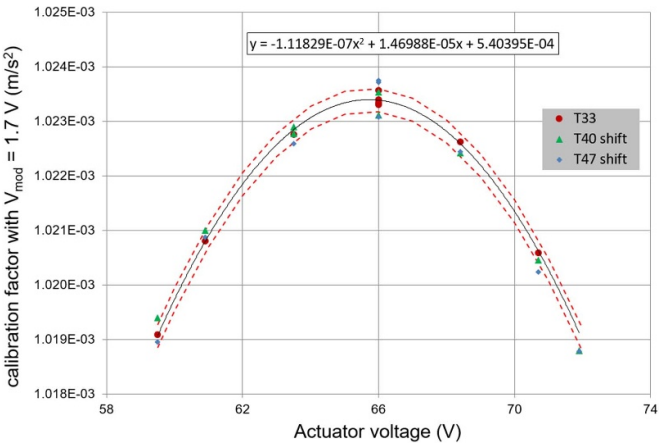

Figure 13. Experimental data of FMx accelerometer obtained at temperatures equal to 40 °C and 47 °C shifted to superimpose to data at temperature equal to 33 °C.

to the temperature set-points. A value of 1600 ppm $°C^{-1}$ is obtained from the best-fit linear regression, with a $R^2 = 0.999$. We can also observe that the curves at different temperatures reported in figure 12 have the same shape and differ only for a vertical shift (i.e. C parameter) which is temperature dependent. So we choose to describe the accelerometer's calibration factor with a model, which is a second order polynomial with respect to the actuator voltage and linear with respect to the temperature. Based on this assumption, with the purpose to estimate the repeatability of the measurements, we can shift the experimental data obtained at temperatures equal to 40 °C and 47 °C to superimpose the central values at 66 V with the central values of data at 33 °C, as shown in figure 13.

The black line in figure 13 represents the curve fitting the data at 33 °C (red dots), whose equation is reported on top of the figure. According to our model, all the 26 data points

displayed in figure 13 belong to the same statistical population, even if obtained at different temperatures. Therefore, we can calculate the residuals of all data from the curve fitting the data at 33 °C. The standard deviation of all residuals has been evaluated equal to 205 ppm (red dashed curves in figure 13). This parameter already includes the contribution of the repeatability at the central point and has been considered as a good estimate for the repeatability of the accelerometers.

The physical model describing the calibration of accelerometers is equation (1), so the main uncertainty components are due to:

- the local gravitational acceleration
- the tilt angle
- the voltage measurement
- the temperature sensitivity
- the calibration repeatability of the accelerometers.

The local gravitational acceleration value, $g_0 = 9.805\ 35\ \mathrm{m\ s^{-2}}$, was measured with the INRIM's absolute gravimeter; the uncertainty $u(g_0)$ has been evaluated equal to $5 \cdot 10^{-6}\ \mathrm{m\ s^{-2}}$, so the relative uncertainty is about 0.5 ppm and is negligible with respect to the other uncertainty components.

The uncertainty of the angle, $u(\alpha)$, is due to the autocollimator calibration performed with respect to the national angle standard [13]. A relative uncertainty $u(\alpha)/\alpha = 1.0 \cdot 10^{-4}$ has been evaluated.

The voltage measurement is based on an ultrastable voltage reference (embedded in the accelerometers electronics) and a ratiometric technique is used for all precise analogue to digital conversions. The end-of-life voltage stability of the actuator plates was evaluated about 2.5 mV by the manufacturer. Thus, considering an average actuator voltage value of 66 V and a uniform probability distribution, a worst case uncertainty contribution due to the voltage measurement equal to 22 ppm has been estimated.

Temperature is a parameter that seriously affects the calibration factor, because of the extremely high thermal sensitivity of the accelerometers. During the calibration, the temperature stability was estimated within ±0.02 °C. Hence, a relative uncertainty contribution equal to 64 ppm has to be added to the uncertainty budget.

The standard deviation of all the residuals from the fitting curve, shown in figure 13, can be considered as a good estimate of the repeatability of accelerometers. So we can assume a relative uncertainty due to the repeatability of all the accelerometers as $u_{\mathrm{rip}}(a)/a = 205$ ppm.

Finally, combining the different uncertainty components, the relative standard uncertainty of the accelerometers calibration has been evaluated as 240 ppm at 1 σ, which for a normal distribution corresponds to a probability of about 68%. The uncertainty contribution due to the reproducibility of the mechanical system was not taken into account in this budget. Indeed, the time slot devoted to the calibration at INRIM was limited by the schedule of the ESA missions. Hence we did not have the possibility to repeat the calibration procedure after dismounting and remounting the device. Anyway, the mechanical stability of these sensors and the repeatability after successive mountings were already investigated during the characterization of the accelerometers performed by the manufacturer.

7. Conclusions

A facility for the calibration of high sensitivity accelerometers developed for ESA missions JUICE and BepiColombo has been set-up. The facility is based on tilting the base of the accelerometer by a known angle α so that the sensor undergoes a component of the gravitational acceleration g proportional to angle α. The procedure makes use of a dynamic analysis in the frequency domain in order to reduce the effect of the seismic background noise. A comprehensive calibration activity was performed in order to test the accelerometer performances under possible different on-flight conditions. A relative accuracy less than 300 ppm, which is the mission requisite, has been achieved.

Data availability statement

The data cannot be made publicly available upon publication because they contain commercially sensitive information. The data that support the findings of this study are available upon reasonable request from the authors

ORCID iD

Milena Astrua https://orcid.org/0000-0001-5713-610X

References

[1] Vielberg K, Forootan E, Lück C, Löcher A, Kusche J and Börger K 2018 Comparison of accelerometer data calibration methods used in thermospheric neutral density estimation *Ann. Geophys.* **36** 761
[2] Visser P N A M and IJssel J A A V D 2016 Calibration and validation of individual GOCE accelerometers by precise orbit determination *J. Geod.* **90** 1
[3] JUICE, European Space Agency (available at: https://sci.esa.int/web/juice) (Accessed 23 June 2023)
[4] BepiColombo, European Space Agency (available at: https://sci.esa.int/web/bepicolombo) (Accessed 23 June 2023)
[5] Iafolla V, Fiorenza E, Lefevre C, Morbidini A, Nozzoli S, Peron R, Persichini M, Reale A and Santoli F 2010 Italian spring accelerometer (ISA): a fundamental support to BepiColombo radio science experiments *Planet. Space Sci.* **58** 300
[6] Fiorenza E, Lucente M, Lefevre C, Santoli F and Iafolla V 2016 Zero-g positioning for the BepiColombo ISA accelerometer *Sens. Actuators* A **240** 31
[7] Santoli F, Fiorenza E, Lefevre C, Lucchesi D M, Lucente M, Magnafico C, Morbidini A, Peron R and Iafolla V 2020 ISA, a high sensitivity accelerometer in the interplanetary space *Space Sci. Rev.* **216** 145
[8] ISO 16063-42 2014 *Calibration of Seismometers with High Accuracy using Acceleration of Gravity* (available at: www.iso.org/standard/43736.html)

[9] Peterson J R 1993 Observations and modeling of seismic background noise *US Geological Survey Technical Report* pp 93–322
[10] D'Alessandro A *et al* 2021 Spectral characterization and spatiotemporal variability of the background seismic noise in Italy *Earth Space Sci.* **8** e2020EA001579
[11] Pisani M *et al* 2015 On-ground actuator calibration for ISA—BepiColombo *IEEE Metrology for Aerospace* (*Benevento, Italy*, *2015*) p 312
[12] Pisani M *et al* 2016 Characterization of ISA—BepiColombo internal calibration source *IEEE Metrology for Aerospace* (*Florence, Italy*) p 495
[13] Pisani M and Astrua M 2017 The new INRIM rotating encoder angle comparator (REAC) *Meas. Sci. Technol.* **28** 045008
[14] Astrua M and Pisani M 2021 Improved performance of a refurbished photoelectric autocollimator *Meas. Sci. Technol.* **32** 015010